We are IntechOpen, the world's leading publisher of Open Access books
Built by scientists, for scientists

6,900
Open access books available

185,000
International authors and editors

200M
Downloads

154
Countries delivered to

Our authors are among the
TOP 1%
most cited scientists

12.2%
Contributors from top 500 universities

BOOK CITATION INDEX
CLARIVATE ANALYTICS
INDEXED

WEB OF SCIENCE™

Selection of our books indexed in the Book Citation Index
in Web of Science™ Core Collection (BKCI)

Interested in publishing with us?
Contact book.department@intechopen.com

Numbers displayed above are based on latest data collected.
For more information visit www.intechopen.com

Radio Frequency Quadrupole Accelerator: A High Energy and High Current Implanter

Yuancun Nie[1,2], Yuanrong Lu[2,*], Xueqing Yan[2] and Jiaer Chen[2]
[1]State Nuclear Power Technology R&D Center, Beijing
[2]State Key Lab of Nuclear Physics and Technology (Peking University), Beijing
China

1. Introduction

In this chapter, issues of applying the radio frequency quadrupole (RFQ) accelerator to ion implantation for material modification and microelectronics will be discussed at first. Subsequently, several examples of the RFQ-based implanters will be introduced, with an emphasis on the ladder IH-RFQ accelerator at Peking University, of which the output beam energy spread is optimized to be much lower than the conventional value by means of a novel beam dynamics design strategy. The chapter is divided into 6 sections, which are the introduction, advantages of RFQ as implanter, problems and solutions of RFQ-based implanters, several RFQs aiming at ion implantation, ladder IH-RFQ at Peking University, and summary.

RFQ accelerator, proposed by I. M. Kapchinsky and V. A. Teplyakov in 1970, can simultaneously focus, bunch and accelerate low energy beam extracted from ion source directly, based on the rf electrical field of a modulated quadrupole transport channel[1]. The details of its principle and development could be found in many literatures[2,3]. Taking advantages of its high current, compact size and good ion selectivity, etc, RFQ has been used widely in the field of particle accelerator, after 40 years' development both in the beam dynamics design and in the rf cavity structure [4]. At present, RFQs can provide high current (up to hundreds mA) ion beams at energy level of MeV over the mass range from Hydrogen to Uranium and the 5 MHz to 500 MHz frequency range[5].

2. Advantages of RFQ as implanter

Many efforts have been made to apply the RFQ accelerator to ion implantation. Generally speaking, the beam line of the RFQ-based implanter consists of the ion source, low energy beam transport (LEBT), RFQ accelerator and the target, equipped with power system, controlling system, vacuum and cooling systems, etc. The advantages of RFQ-based implanter are concluded as follows:

- The beam extracted from the ion source is accelerated further by the following RFQ, so the beam energy can reach the order of several MeV, which fulfills the requirement of deep deposition.

---

[*] Corresponding Author

- The current of heavy ion beam accelerated by the RFQ could be in the mA-range. For an implant dose of 10^{18} ions/cm^2, the implantation time needed is less than 3 minutes/cm^2 using an ion beam with average current density of 1 mA/cm^2.
- RFQ can simultaneously accelerate positive and negative ions with the same charge to mass ratio[6]. It makes full use of the rf power, and more importantly it avoids the charge accumulation while doubling the implant flux density.
- For a given RFQ, it is available not only for the designing ion beam, but also for other ion species, as long as the injection energy and the inter-electrode voltage are adjusted appropriately. For example, the 36 MHz IH-RFQ in the UNILAC accelerator of GSI can accelerate all the heavy ions with charge to mass ratio greater than 1/65 from 2.2 keV/u to 120 keV/u[7].
- Compared to the electrostatic accelerator, high voltage breakdown and high energy X-ray radiations are reduced greatly for this case, because high voltage terminal is avoided and the rf inter-electrode voltage in RFQ is normally below 100 kV.
- The equipment is very compact. For instance, the 26 MHz ISR-1000 RFQ at Peking University can accelerate $^{16}O^+$ beam from 22 keV to 1 MeV within 2.6 m, and the cavity diameter is 0.75 m[8].

3. Problems and solutions of RFQ-based implanters

The RFQ-based implanter has some drawbacks, i.e. the output beam energy is normally fixed for a given RFQ, and the output beam energy spread is quite big (usually the full width at half magnitude, FWHM energy spread is around 3%).

To make the output beam energy variable, two methods have been used, and they are:

- Making the resonant frequency of the RFQ cavity variable. It is mostly applied to the 4-rod RFQs. For instance, at Frankfurt University several VE (Variable energy) RFQs have been developed, and the output energy range could be doubled and even more while the ground plate connected to the stems is moved to vary the frequency (VF)[5]. Hitachi Ltd. also invented a variable energy RFQ linac with an external tunable one-turn coil, and the variable resonant frequency range is from 9.6 to 39 MHz, which corresponds to an energy variation of 16 times[9].
- Changing the output energy by using a high voltage platform (HVP) or a Spiral Loaded Cavity (SLC). The variation in the beam energy is continuous in the range determined by the HVP, for example in Ref.[10], the 60 MHz RFQ implanter with the HVP at voltage higher than 250 kV could provide a beam energy variable from 500 keV to 1.5 MeV for ions with charge to mass ratio 2/16. At Frankfurt University, a SLC was coupled to the RFQ designed for the acceleration of N$^+$ from 50 keV to 1.5 MeV to vary the beam energy in a range of ±200 keV[11].

To reduce the output energy spread, non-adiabatic bunching method could be used and there are also two ways:

- The first one is the external bunching method. A beam dynamics design with energy spread 0.6% has been realized for $^{14}C^+$ beam using this method[12]. However, the pre-buncher used to produce a pulsed beam from a DC beam before the RFQ makes the system complex, and the total beam transmission efficiency is constrained by it.
- The second one is the internal discrete bunching method. Most recently, the low energy spread beam dynamics design for ions with charge to mass ratio greater than 1/14 was

accomplished[13]. Optimization procedure of the design as well as its preliminary beam experiment will be discussed in detail.

4. Several RFQs aiming at ion implantation

In the following Table 1, parameters of several typical RFQs for ion implantation in the world are summarized.

Affiliation	RFQ structure	Ions or charge-to-mass ratio	Energy (MeV/u)	Current (mA)	Frequency (MHz)	Length (m)	Note
GSI	Split coaxial	Ar^+,Kr^+	0.045	5	13.5	9.4	Operation
Hitachi	Inductance-Capacitance	P^+,N^+	0.043	5	17.3	2.3	Operation
Hitachi[9]	4-rod	1/31	0.036	1	21	2.3	VE(VF)
Peking University	Integral Split Ring	O^+,O^-, N^+	0.0625	0.5	26	2.6	Operation
Nissin	4-rod	B^+,N^+,O^+	0.0835	0.2	33.3	2.22	Operation
Seoul[10]	Modified 4-vane	2/16	0.0625±0.0313	2	60	1.57	VE(HVP)
Simazu	4-vane	B^+,N^+,P^+	0.09	0.1-0.4	70	2.1	Operation
Frankfurt	4-rod	B^+	0.09	15	81	1.2	Operation
Frankfurt[11]	4-rod	1/14	0.107±0.014	10	108.5	2.0	VE(SLC)

Table 1. Parameters of some RFQs for ion implantation (after Ref.[14])

5. Ladder IH-RFQ at Peking University

Since the year 2008, a 104 MHz ladder type IH-RFQ has been developed at Peking University, for the acceleration of the ion species with mass-to-charge ratio smaller than 14 from 2.86 keV/u to 35.71 keV/u. As a specific feature, the output beam energy spread is as low as 0.6% achieved through the internal discrete bunching method, which makes potential applications of the RFQ feasible, such as accelerator mass spectrometry (AMS) and ion implantation. Design procedures and the most recent experimental results of the ladder IH-RFQ will be described in detail.

5.1 Beam dynamics design of the ladder IH-RFQ

In recent years, RFQ based ^{14}C AMS application has been studied extensively at the Institute of Heavy Ion Physics (IHIP), Peking University. Great efforts have been made to reduce the output FWHM energy spread of the RFQ. Non-adiabatic bunching method could be used owing to the lack of space charge effect since the current is usually weak. A beam dynamics design with energy spread 0.6% has been realized by means of the external bunching method. However, the total beam transmission efficiency is constrained by the pre-buncher used to produce a pulsed beam before it is injected into the RFQ. For this reason, we tried another possibility, the internal discrete bunching method proposed by J. W. Staples at LBNL to reduce the output energy spread without the pre-buncher[15]. The final low energy spread beam dynamics design for $^{14}C^+$ RFQ was accomplished. Optimization procedure of the design along with its performances will be reported.

The operating frequency 104 MHz was chosen because of the limitation of the existing rf power transmitter, and our interest of investigating the ladder type IH-RFQ structure [13], in which the four electrodes are supported alternately by erect stems mounted to the external cavity from top to bottom equidistantly, different from the traditional 4-rod RFQ and IH-RFQ structures. Properties of the ladder IH-RFQ will be studied in the next section.

According to the strategy of the internal discrete bunching, the whole RFQ beam dynamics design is divided into five sections, different from the conventional four-step method developed at LANL [16], consisting of the radial matcher, the buncher section, the drift section, the transition section and the acceleration section. With the buncher and drift sections serving as an internal non-adiabatic buncher, the new method reduces the output longitudinal emittance significantly and transverse emittance slightly compared with the traditional one. However, neither this strategy nor the conventional method takes into account the match between the beam size and the acceleration channel carefully, leading to beam envelope mismatch and even particle loss. According to the beam matching equation for weak current

$$\varepsilon_{tn}^2 = \frac{a_0^4 \gamma^2 \sigma_t^2}{\lambda^2} \tag{1}$$

where ε_{tn} is the normalized rms (root mean square) emittance, a_0 is the transverse rms beam radius, γ is the relativistic gamma, λ is the rf wavelength, and σ_t is the transverse phase advance without current. σ_t can be obtained by solving the transverse motion equation, i.e. the Mathieu Equation, and we have

$$\sigma_t^2 \propto \frac{B^2}{8\pi^2} + \Delta \tag{2}$$

where B is the focusing parameter for the RFQ accelerator, while Δ is the defocusing factor, which are defined as follows

$$\Delta = \frac{qe\pi^2 A V \sin\varphi_s}{2m_0 c^2 \beta_v^2 \gamma}$$

$$B = \frac{qe\lambda^2 F V}{m_0 c^2 a^2 \gamma} \tag{3}$$

where A, V, φ_s, F are the acceleration coefficient, inter-electrodes voltage, synchronous phase and focusing factor, respectively, β_v is the relativistic velocity, a is the minimum aperture radius between two opposite electrodes of one acceleration cell. Based on the matching design method [17], we enhance the focusing parameter B gradually as the defocusing factor $|\Delta|$ increasing due to the growing acceleration coefficient A, during the first stage of the transition section that serves as the shaper section in the four-step method. Nevertheless, in the acceleration section, B is decreased slowly since $|\Delta|$ is reduced because of the rapidly increasing beam energy. The above improvements make the transverse phase advance σ_t constant, thereby the beam matched, accordingly suppress the emittance growth and minimize the particle loss.

In addition, there is an approach to reduce the RFQ energy spread furthermore, which can be shown by

$$\Delta w_{\max} = \left[2\xi eAVW_s \left(\varphi_s \cos \varphi_s - \sin \varphi_s \right) \right]^{1/2} \tag{4}$$

where $\Delta w_{\max}$ is the separatrix height that indicates the maximum beam energy spread, ξ is the charge-to-mass ratio q/A_0 of the ion, e is the charge of an electron, and W_s is the kinetic energy of the synchronous particles. It can be seen that the energy spread can be reduced by decreasing A and the inter-electrode voltage V while increasing the synchronous phase φ_s, where lower A means lower electrode modulation m. It means that φ_s should be as large as possible even close to 0° at the last acceleration cell in order to achieve low energy spread, not necessarily be -30° as usual. For our case, the frequency 104 MHz is relatively high for ^{14}C ions with $q/A_0=1/14$, which destines a small aperture radius a in order to obtain sufficient focusing strength under a certain V. Small aperture radius means small electrode-tip radius r_0 to avoid excessive Kilpatrick coefficient[2]. To relax the manufacture pressure of the electrodes, we have to enhance V to increase a, unfortunately, it conflicts with reducing not only the energy spread but also the power consumption. As a result of the compromise, an inter-electrode voltage 60 kV is used.

The main parameters were generated by the matched and equipartitioned design code MATCHDESIGN developed at IHIP[17], while the non-adiabatic buncher section was designed by the code of Staples[15]. Beam transport simulation was performed by the program RFQDYN derived from PARMTEQ[16]. In order to make a as large as possible, we tried to reduce B during the transition section and the acceleration section while ensuring the balance between defocusing and focusing of the beam. It finally induced 2% particle loss at the transverse direction. The final value of the synchronous phase φ_s was set to be -6° at the end of the acceleration section, which decreased the output beam energy spread and additionally quickened the acceleration process. The modulation parameter m was also evolved carefully, in view of that large modulation is advantageous to particle acceleration, but disadvantageous to reducing the energy spread.

Figure 1 shows us the evolutions of the focusing parameter B as well as the acceleration coefficient A along with the cell number for the final beam dynamics design. The other
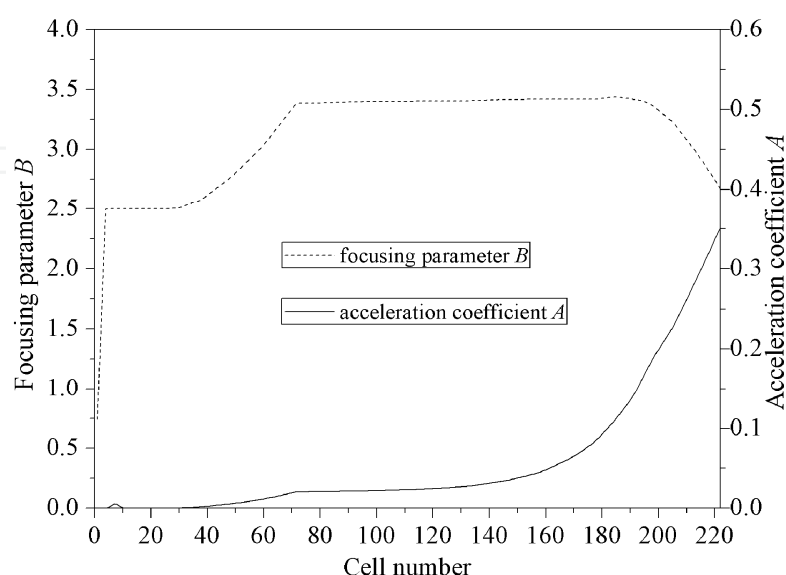

Fig. 1. Variations of the focusing parameter and the acceleration coefficient with the cell number of the ladder IH-RFQ.

dynamics parameters of the RFQ are plotted in Fig. 2. The rapidly advance of φ_s leads to a small portion of particles lose their balances of the longitudinal motion and can't be accelerated effectively. This explains why a tail appears in either the output energy spectrum or the output phase spectrum. The resultant transmission is 97.6%, while 80% particles are in the phase range of ±15° around φ_s, and 90% for ±30°. Meanwhile, more than 90% particles are limited by the energy range ±15keV, with the FWHM energy spread 0.6%. The total length of the electrode is about 1.1 m to accelerate the $^{14}C^+$ beam from 40 keV to 500 keV, which is supposed to be slightly longer than that of the external bunching method due to the implanted non-adiabatic buncher. In view of the overall simplified system and much higher transmission efficiency in total, the internal non-adiabatic bunching strategy is a competent candidate to design the RFQ for AMS application.
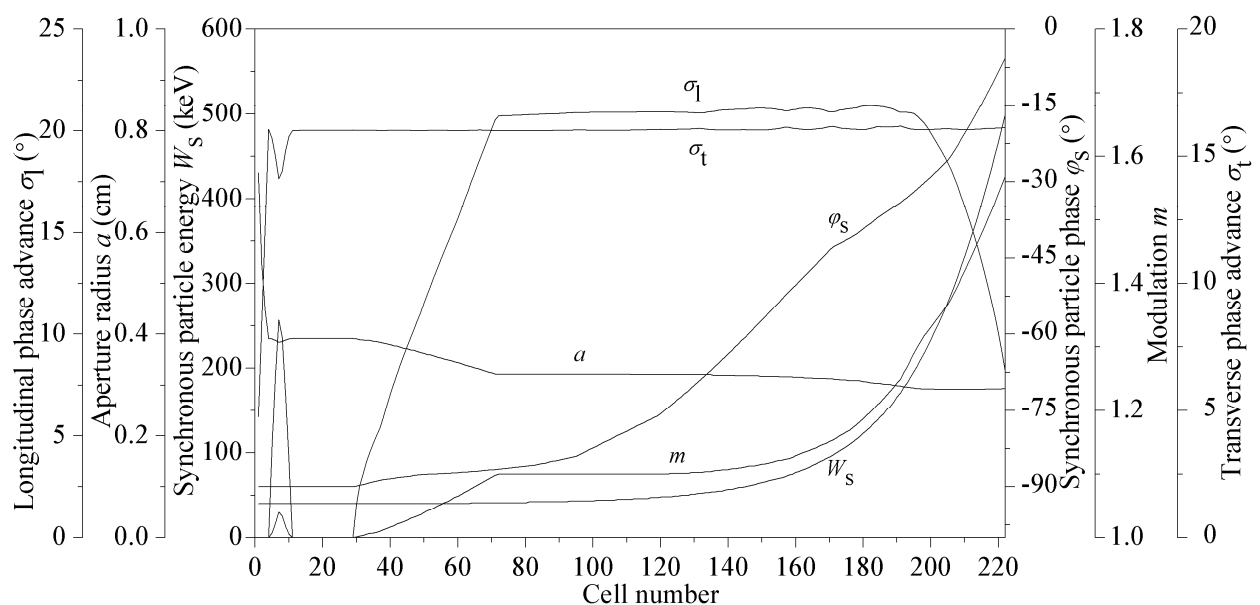
Fig. 2. The main beam dynamics parameters varying with the cell number of the ladder IH-RFQ.

Responses of the beam transmission efficiency and the output beam energy spread to input Twiss parameters (a, β), current and emittance (normalized, rms) are presented in Fig. 3, with the design values (0.31, 2.19 cm/rad), 0 mA, 0.042 mm-mrad, respectively. Figures 3(a) and 3(b) illustrate that neither the beam transmission efficiency nor the output beam energy spread is sensitive to the Twiss parameters, since all the fluctuations are acceptable within the plotted ranges. The influences of the input emittance on the transmission efficiency and output energy spread are observed but tolerable considering that even when it is twice the design value, the transmission efficiency and energy spread are still higher than 90% and below 1.5%. A remarkable feature is that the transmission efficiency and energy spread are better than 93% and 0.8% at the current 1 mA, despite the beam dynamics was optimized at 0 current.
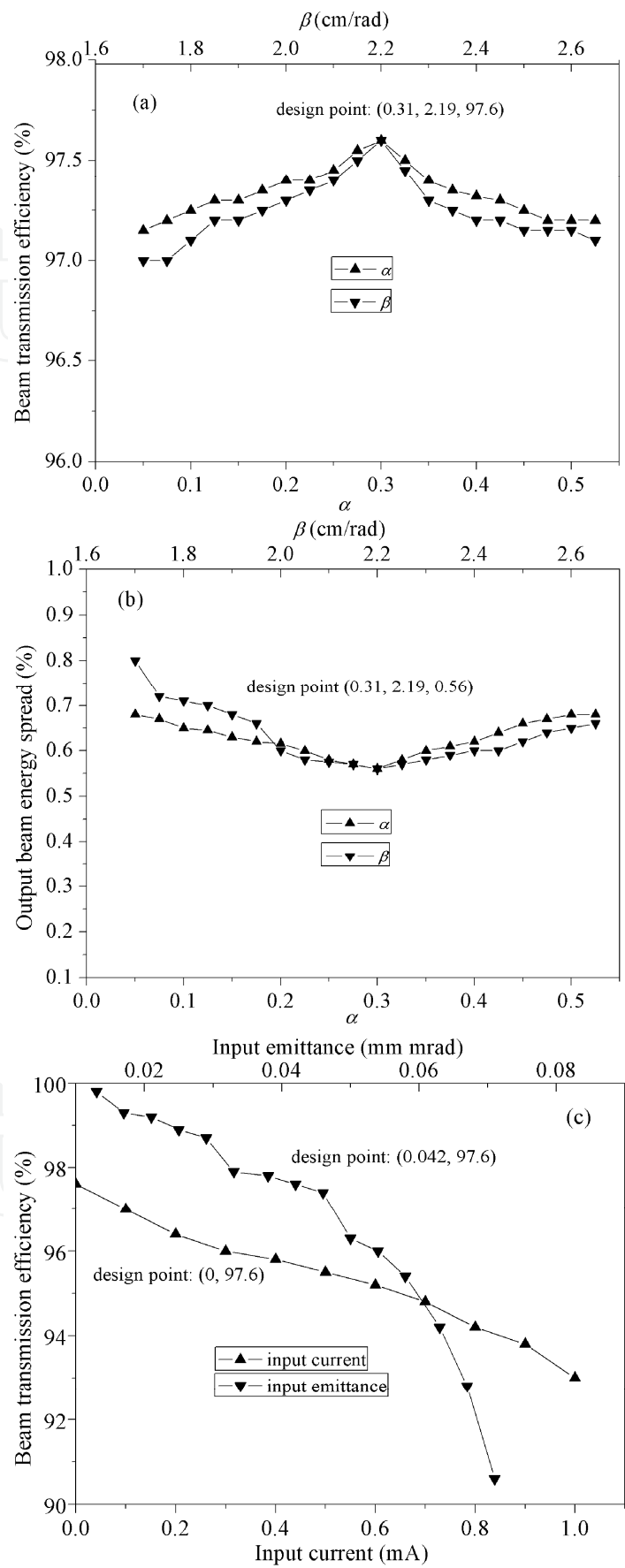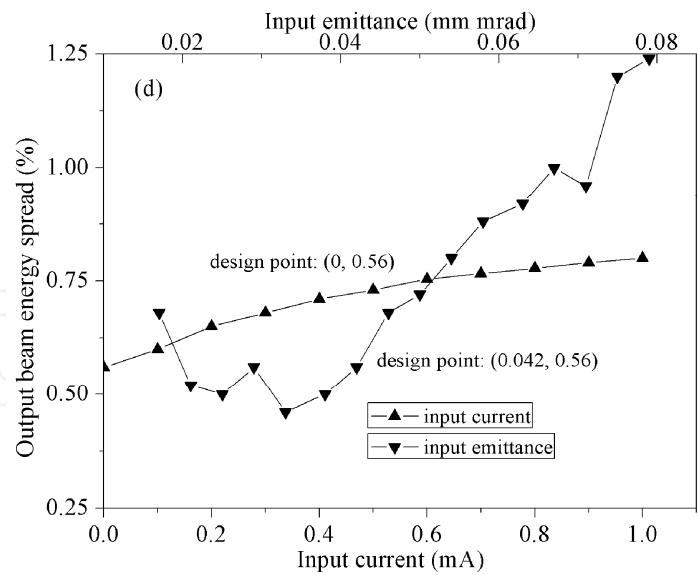
Fig. 3. Stability studies of the beam dynamics design of the ladder IH-RFQ: beam transmission efficiency versus Twiss parameters in (a), output beam energy spread versus Twiss parameters in (b), beam transmission efficiency versus input current and emittance in (c), output beam energy spread versus input current and emittance in (d).

The design has been proved to be suitable for various ion species with different charge-to-mass ratio q/m_0 and even different frequencies, as long as the operating parameters are chosen appropriately. According to (3), it can be seen that the focusing strength B is proportional to q/m_0, λ^2 and V. Meanwhile, the length of one acceleration cell is $\beta_v\lambda/2$. For given electrodes structure, when q/m_0 or λ changes, V and β_v i.e. the injection energy $W_i=1/2m_0v^2$ should be adjusted to keep B and the injection cell length unaltered, hence achieve the matching between the acceleration channel and the input beam. The beam dynamics parameters are listed in Table 2.

Ion species	$^{14}C^+$	$^{13}C^+$	$^{12}C^+$	$^{4}He^+$	$^{4}He^+$	$^{4}He^+$
Frequency f (MHz)	104	104	104	104	100	106.4
Inter-electrode voltage V (kV)	60	55.7	51.4	17.1	15.9	17.9
Injection energy W_i (keV)	40	37.1	34.3	11.4	10.6	12.0
Output energy W_{out} (keV)	500	464	428	143	132	150
Transmission T (%)	97	97	97	97	97	97
Energy spread (%)	0.6	0.6	0.7	1.0	1.1	1.0

Table 2. Beam dynamics parameters of the ladder IH-RFQ

5.2 RF design of the ladder IH-RFQ

According to the above beam dynamics design, the average electrode-tip radius is 3.1 mm corresponding to the average aperture radius 3.5 mm. Figure 4 shows the resonant model of CST Microwave Studio (MWS)[18] simulations for the ladder IH-RFQ. Simulation results of the electromagnetic field validated that the ladder IH-RFQ operates at $H_{21(0)}$ mode. As a consequence, the resonant frequency of it is unsurprisingly more than two times that of IH-

RFQ and about 1.3 times that of 4-Rod RFQ under the same transverse dimension, making it very attractive at frequencies above 100 MHz. Moreover, in respect that the electrodes are supported by completely symmetric stem structures, the quadrupole field of the ladder IH-RFQ is ideal unlike the 4-Rod RFQ and IH-RFQ, the dipole components of which are typically 2-3% and 0.5%, respectively[19].

Fig. 4. MWS simulation model of the ladder IH-RFQ.

Many authors have reported their studies on the RFQ cavity modeling[20,21]. The conventional electrical model are shown in Fig.5, consisting of the equivalent resistance, inductance, capacitance and parallel shunt impedance, denoted by R, L, C and R_p, respectively. According to the definitions of intrinsic quality factor $Q_0 = \omega W / P$ and shunt impedance $R_p = V^2 / P$, with the resonant frequency $\omega = 2\pi f = 1/(LC)^{1/2}$, average energy stored in one period $W = 1/2 I^2 L = 1/2 C V^2$ (where I is peak current and V is peak voltage), and power dissipation $P = 1/2 I^2 R$, we have

$$Q_0 = \frac{1}{R}\sqrt{\frac{L}{C}} = \frac{R_P}{2}\sqrt{\frac{C}{L}} \tag{5}$$

For RFQ cavity having N basic resonant cells, the relation between the total R, L, C, I and the corresponding values of one cell R_{cell}, L_{cell}, C_{cell}, I_{cell} will be

$$I = NI_{cell} \ , \ C = NC_{cell} \ , \ L = L_{cell}/N \ , \ R = R_{cell}/N \tag{6}$$

when ignoring the end effect. Combining (5) with (6) we find

$$Q_0 = Q_{0,cell} \ , \ R_p = R_{p,cell}/N \tag{7}$$

where cell denote the values of single cell. For ladder IH-RFQ, Fig.6 shows the simplified circuit of one cell with

$$C_{cell} = 2C_{stem} + C_{rod} \ ; \ L_{cell} = L_{stem}/2 \ ; \ R_{cell} = R_{stem}/2 \tag{8}$$

In (8) it is assumed that the resistance and inductance are mainly attributed to the stems, while the capacitance arises from the two pairs of opposite electrodes and adjacent stems with C_{rod} several times greater than C_{stem} generally.
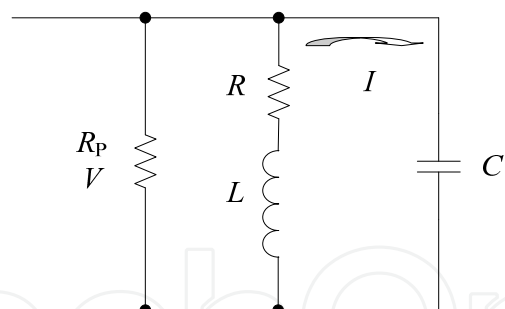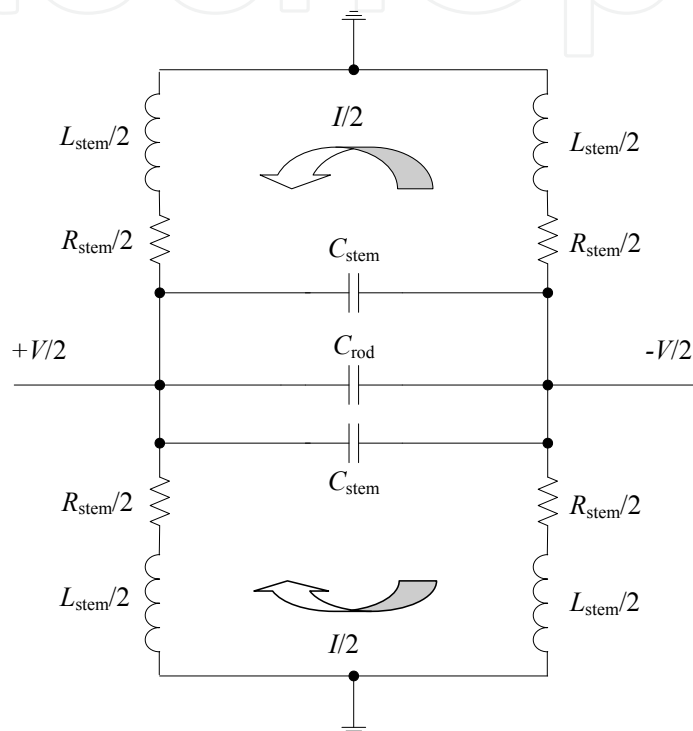
Fig. 5. Equivalent circuit of RFQ cavity.

Fig. 6. Equivalent circuit of single cell for the ladder IH-RFQ.

Based on the equivalent circuit analysis, table 3 lists the MWS-simulated rf properties of different RFQ structures at the same transverse size, which is in agreement with the theoretical predictions.

RFQ Structures	Frequency (MHz)	Shunt impedance (kΩ)	Quality factor	The first High-mode Frequency (MHz)
IH-RFQ	46.5	273	5934	137.2
4-rod RFQ	77.9	155	5077	143.9
Ladder IH-RFQ	103.6	100	5192	156.3

Table 3. Comparison of different RFQ structures at the same transverse size

Mode analysis of the RFQ was performed using the eigenmode solver of MWS. Fig. 7 shows the electric field, magnetic field and surface current distribution. It can be seen that the two parts of inductance and resistance of one stem are in parallel. These results agree with the electromagnetic field distribution of a H_{210} mode, and the expectation from Fig.6.
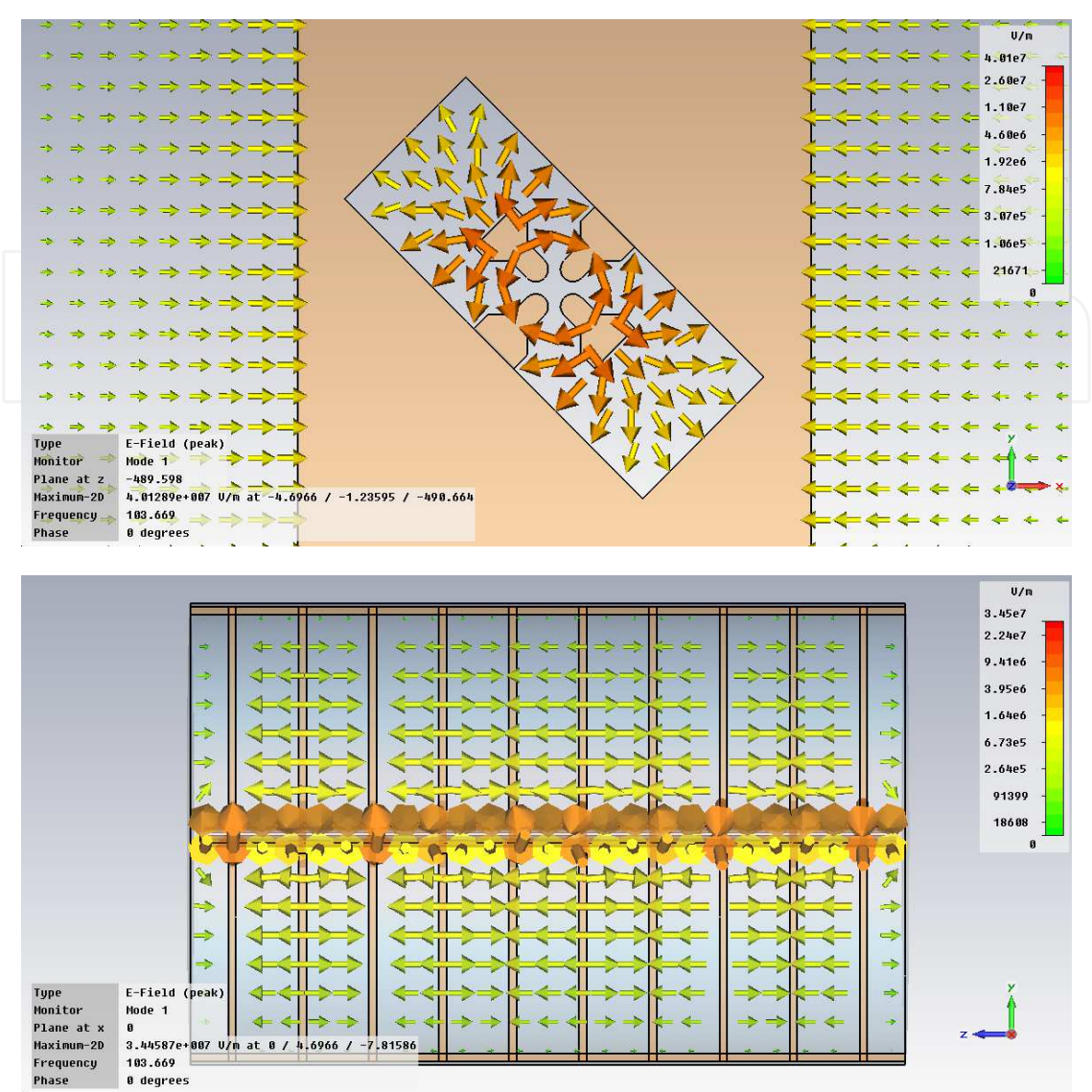
(a) Electric field among electrodes (up) and stems (bottom) of the ladder IH-RFQ
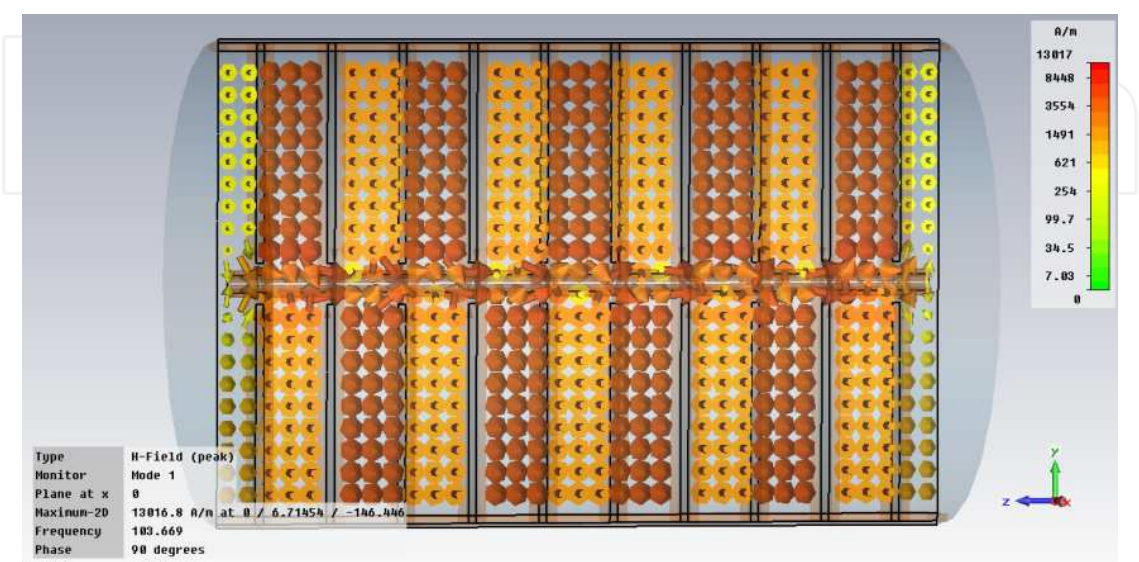
(b) Magnetic field distribution of the ladder IH-RFQ
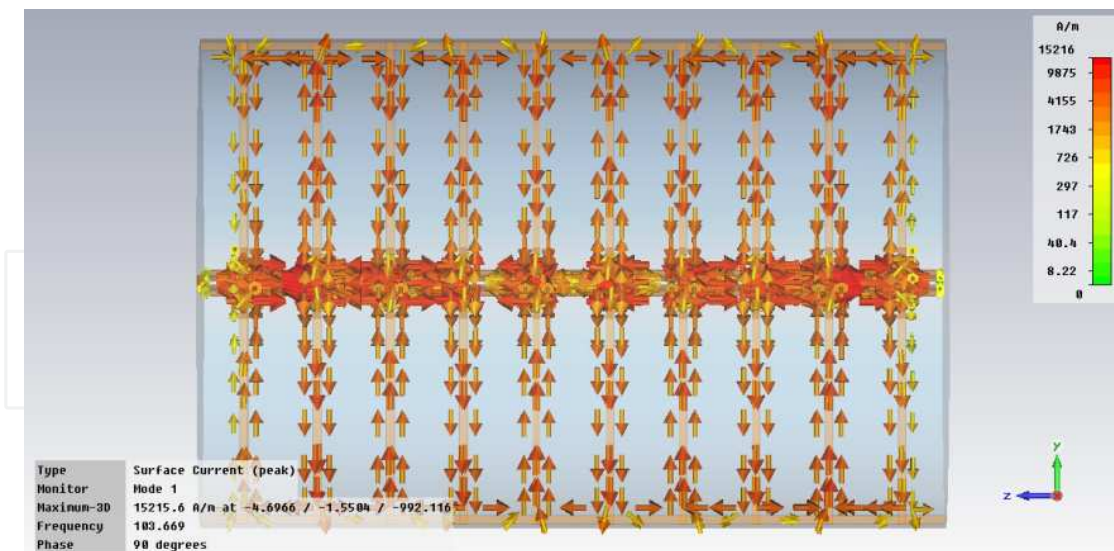
(c) Surface current flow of the ladder IH-RFQ

Fig. 7. MWS-simulated results of the electromagnetic field and surface current flow of the ladder IH-RFQ.

The RFQ structure was optimized by parameter sweeping to find the maximum Q_0, R_p, and minimum P at 104 MHz. Some conclusive results are as follows.

1. Stem number N_{stem}: The beam dynamics design established the inter-electrodes aperture and the electrode length, therefore the first parameter to be studied is the stem number N_{stem} used. Bigger N_{stem} means shorter distance between adjacent stems d, leading to decreasing L_{cell} and C_{cell}, but slightly increasing R_{cell} in view of more serious proximity effect. Taking (6) into account, R, L will decrease while C increase because of the increment in C_{stem}, finally resulting in bigger f as illustrated by MWS simulations. The cavity diameter D has to be scaled to keep f 104 MHz. Fig.8 shows the relevant simulation results, according to which 10 stems was employed.
2. Cavity diameter D: As a variable D is always used to make f unaltered when sweeping the other parameters. When f needs to be lowered, D should be extended to make L_{stem}, C_{stem} as well as R_{stem} bigger.
3. Stem spacing d: Over the 95 mm to 115 mm d range in 5 mm increments with $N_{stem}=10$, f decreases while R_p and Q_0 increase due to smaller C_{stem}, R_{stem} and bigger L_{stem} with increasing d. After adjusting D, it was found that R_p and Q_0 are approximately proportional to d, taking into account the end effects and the mechanical feasibility $d=110$ mm was eventually chosen.
4. Stem width W_{stem}: The increase in C_{stem}, and decrease in L_{stem} as well as R_{stem} with W_{stem} over the simulation range result in increasing f and Q_0 but decreasing R_p. By adjusting D, it could be seen that there is a peak value of R_p, this is why $W_{stem}=130$ mm was adopted to make power loss least.

The inter-electrodes voltage is usually supposed to be constant longitudinally when carrying out the beam dynamics design. So it has long been an important topic that how to tune the voltage unflatness of the RFQ owing to the end effect and modulated electrodes to ensure a good beam quality. For the ladder IH-RFQ, adjustable tuning plates as shown in Fig.4 can be inserted into two neighboring stems symmetrically up and down, which is similar to the case of the 4-Rod RFQ[22]. The tuning plates serve as short pieces of stems, changing their

inductances thus the frequency and field strength. To verify their tuning capability, corresponding simulations were performed for different tuning plate heights 0, 50 and 100 mm, of which the results are plotted in Fig.9. Here electric field is equal to the voltage between relevant electrodes, since the electrodes are unmodulated with uniform aperture radius. It can be seen that the field unflatness achieves its optimum value 2% when the tuning height is 100 mm. Tuning plates cause increment in the eigenfrequency of RFQ, so f is generally set to be several percents lower than the desired value to leave enough tuning space.

(a) structure parameters

(b) rf properties
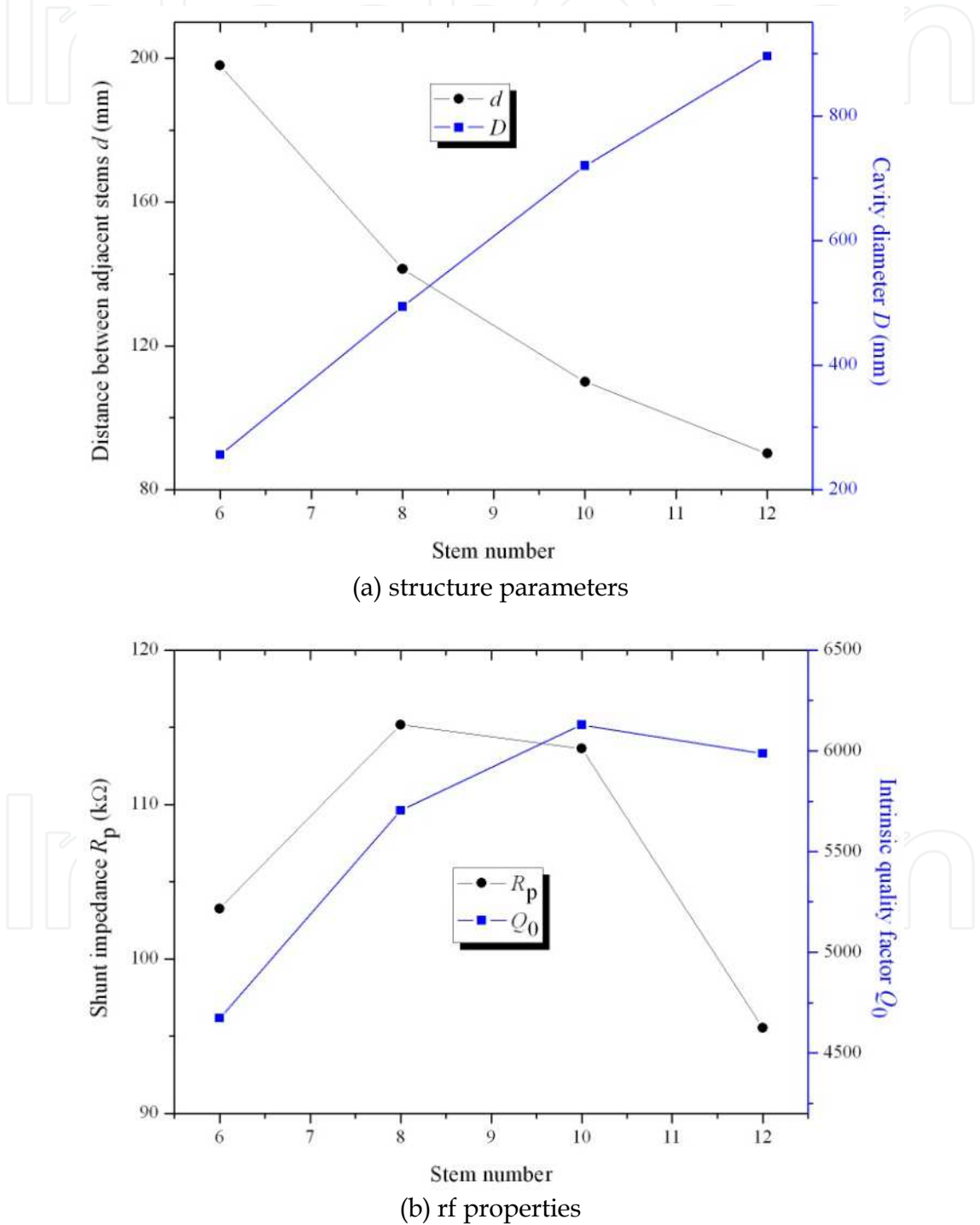
Fig. 8. Variations of the ladder IH-RFQ parameters with stem number.
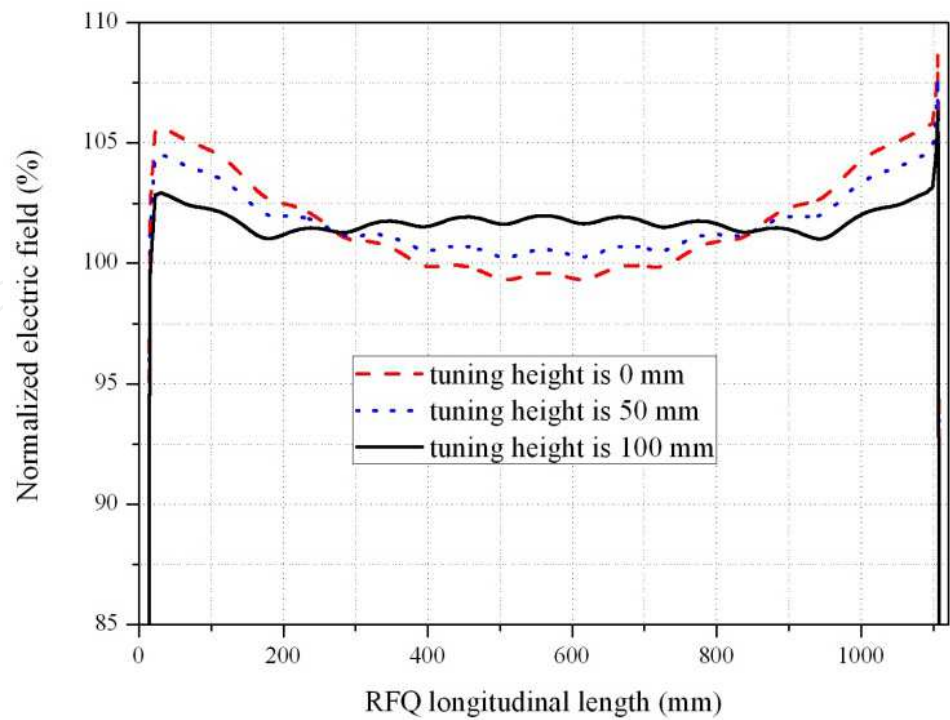
Fig. 9. Variations of the field unflatness with tuning plates height of the ladder IH-RFQ.

5.3 Experimental studies on the ladder IH-RFQ

The constructed ladder IH-RFQ cavity is shown in Fig.10. The geometrical parameters are as follows: the cavity is 720 mm in diameter and 1123 mm in length; 10 supporting stems with width and spacing of 130 mm and 110 mm, respectively, are used. The stems are mounted on two fixing plates up and down to improve the mechanical performance and in the

Fig. 10. The constructed ladder IH-RFQ cavity.

interest of installation. The stems and plates are made of oxygen free copper, and there are water-cooling channels in them. The inner wall of the cavity tank is well plated with copper of more than 0.1 mm in thickness to improve the rf performances. In order to fix the stems and plates on the tank, four copper blocks with tuning thickness 30 mm are used, which will make the resonant frequency higher and improve the field unflatness at the same time.

On the basis of transient simulations with MWS, a magnetic coupling loop with size of about 90 mm×50 mm in between two neighboring stems was established for rf power feeding of the ladder IH-RFQ. The critical coupling condition was met after proper adjustment of the loop orientation, and the result is shown in Fig.11(a). The cold measurement was performed by means of a vector network analyzer and the capacitance perturbation method. S-parameters were measured using an Angilent 8753E network analyzer, and the loaded quality factor Q_L was obtained by 3 dB method. Consequently, the unloaded or intrinsic quality factor Q_0 could be computed using $Q_0 = Q_L(1 + \beta_c)$, where the coupling factor β_c is defined as Q_0/Q_e with the external quality factor Q_e. During the experiment, a very small pick-up loop was used to weaken the influence of it on the cavity properties, as a result, $\beta_c \approx 1$ for critical coupling, i.e. $Q_0 = Q_e$. Referring to the shunt impedance, the perturbation capacitor method was adopted as described in Ref.[23,24]. According to the definitions of intrinsic quality factor $Q_0 = \omega W/P$ and shunt impedance $R_p = V^2/P$, we have

$$R_p = \frac{2Q_0}{\omega C} \tag{9}$$

When using a perturbation capacitance ΔC, the perturbed resonant frequency of the cavity f_{per} becomes

$$f_{per} = \frac{1}{2\pi\sqrt{L(C + \Delta C)}} \tag{10}$$

So the effective capacitance of the cavity can be thus obtained by

$$C = \frac{\Delta C}{\left(f / f_{per}\right)^2 - 1} \tag{11}$$

Finally R_p is calculated using (9), and the square root of it is treated as the relative value of the inter-electrode voltage. The locations of the perturbation capacitor are moved from stem to stem as shown in Fig.11(b), in the interest of the average R_p and voltage unflatness. Figure 12 is the adjustment result of the feeding point, and Fig.13 shows the S_{21} parameter with the loaded quality factor 1861 at 106.7 MHz. The cold measurement result of the shunt impedance is 102 kΩ compared with the simulation value 110 kΩ. The measured inter-electrode voltage unflatness and the simulated result are compared in Fig.14.

Finally, the high-power test and beam test of the ladder IH-RFQ were performed[25]. The rf and measurement system of the experiment is plotted in Fig.15. We used one pulse generator to control the ECR source[26] and the rf transmitter at the same time. The rf power is provided by the FM Transmitter, 816R-4, operating in the 88~108 MHz frequency range with the maximum rf output of 27.5 kW, the excitation of which is from a CE 802A solid-

state FM wideband exciter. The input signal of the exciter is given by a signal modulation system consisting of a CW signal source, the pulse generator, a high frequency (HF) switch and a 30 dB solid-state power amplifier. The output of the transmitter is applied to the RFQ cavity via a low-pass filter and directional coupler. The beam current was measured using Faraday cups with the help of standard pick-up resistances.
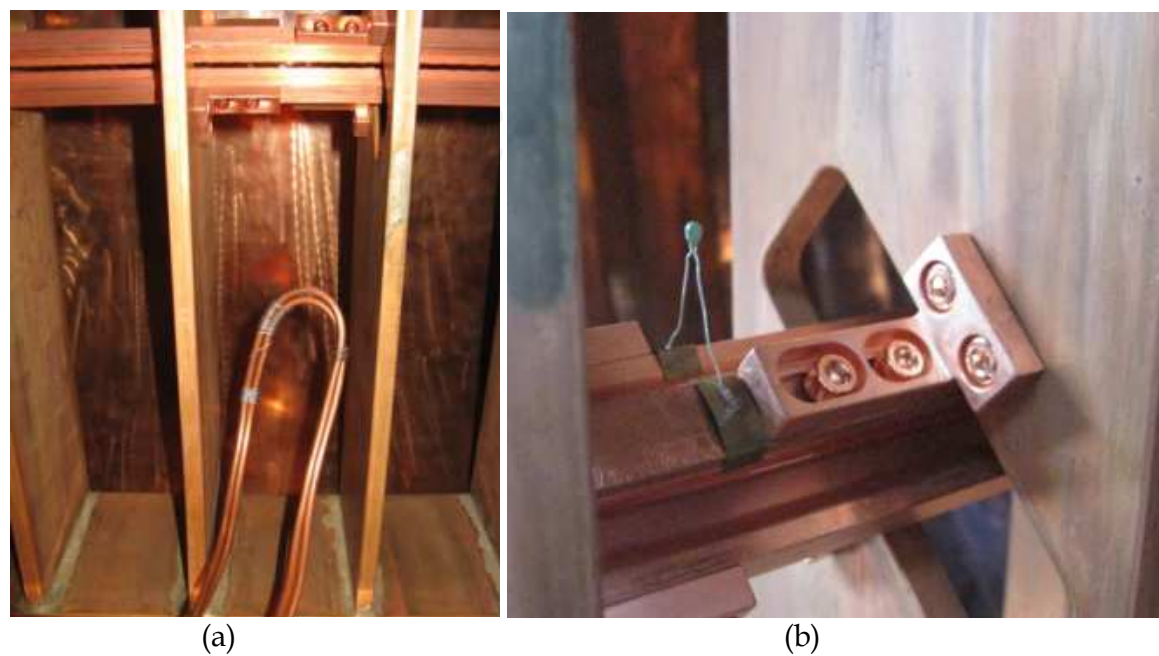

(a)   (b)

Fig. 11. The critical coupling loop (a) and the perturbation capacitor (b) of the ladder IH-RFQ.
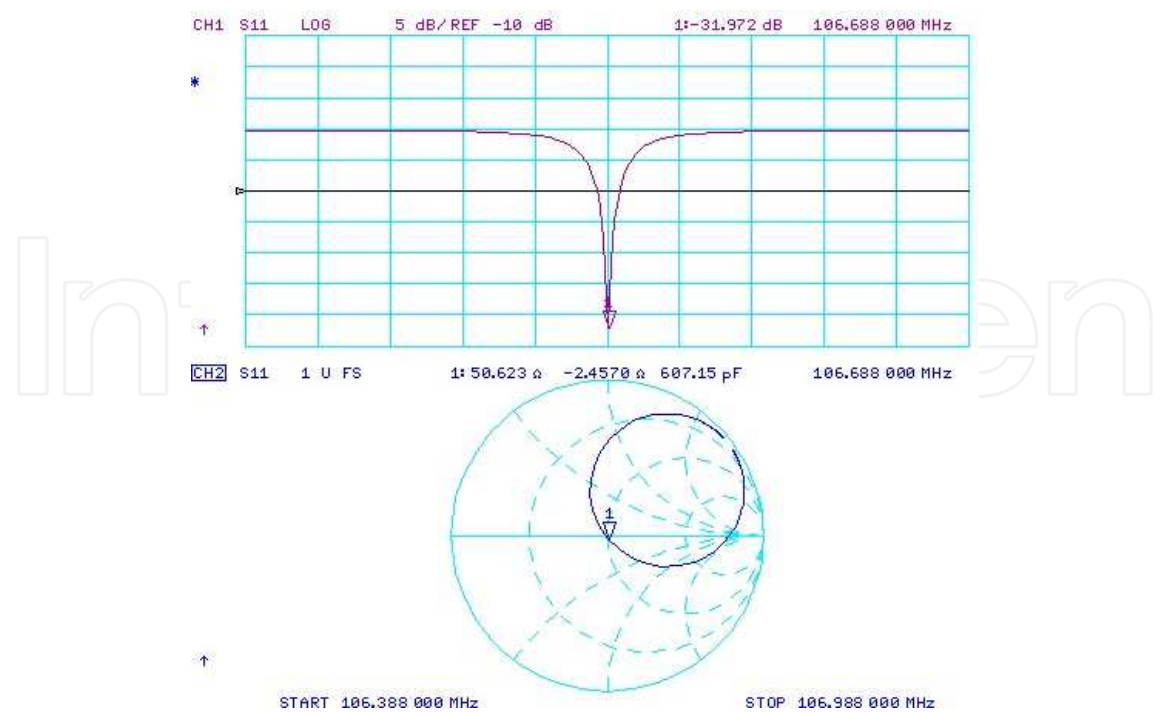
Fig. 12. The critical coupling point of the ladder IH-RFQ: the S_{11} parameter (up) and Smith Chart (down).
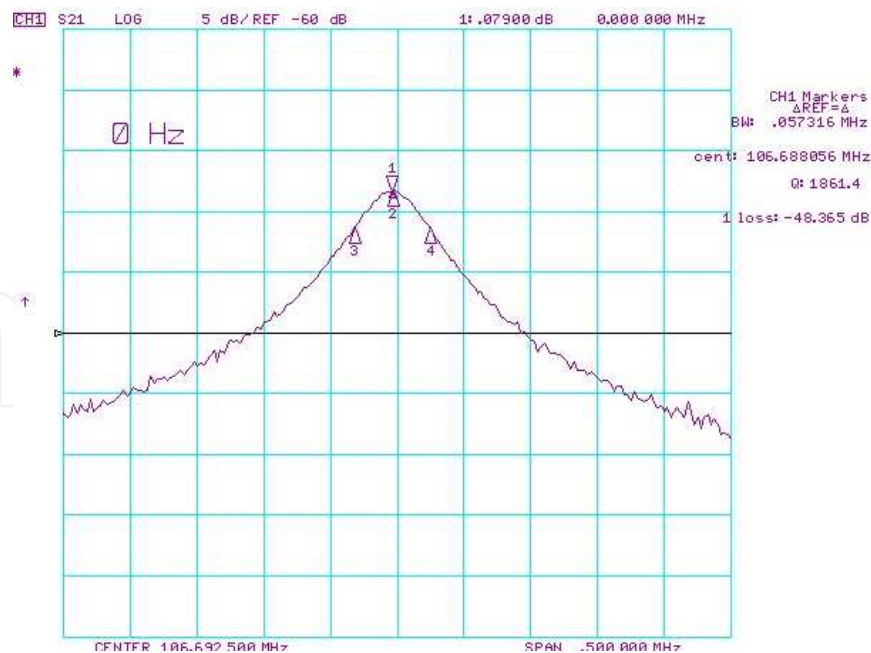
Fig. 13. The measured S_{21} parameter of the ladder IH-RFQ.
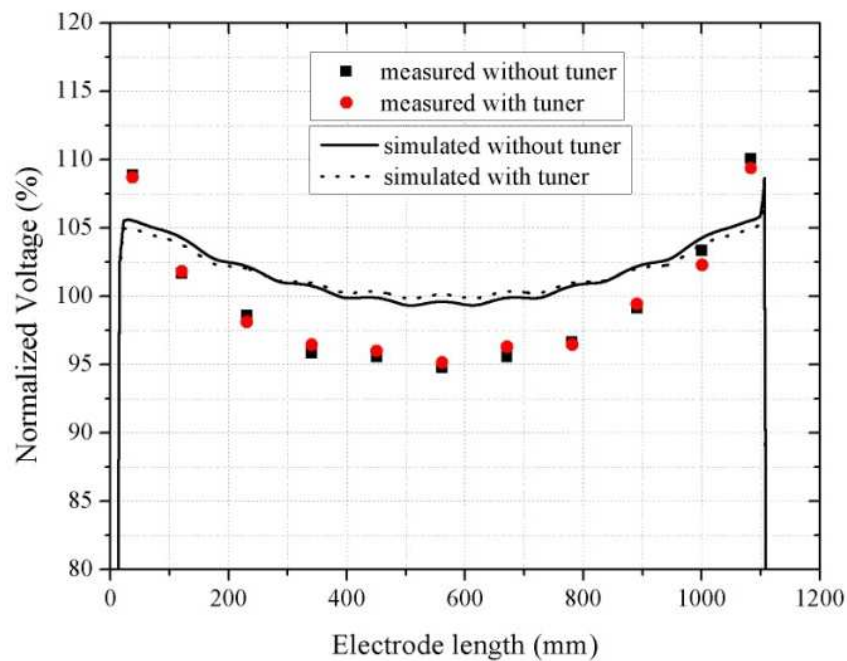
Fig. 14. Simulated and measured voltage unflatness of the ladder IH-RFQ.

Commissioning of the transmitter was carried out at first, because it had been more than 10 years since the last operation. During the experiment, a water load with 50 Ω impedance was used to consume the rf power from the transmitter. The inter-electrode voltage was started to be measured when the high vacuum in the RFQ cavity reached 10^{-5} Pa with both cooling water and high rf power. To obtain the inter-electrode voltage, a high purity Ge detector cooled by liquid nitrogen was used to measure the energy spectrum of X-ray [8]. An ORTEC computer multi-channel system was employed to deal with the signal, which consists of a preamplifier, a master amplifier, a PCI computer multi-channel card and a

notebook PC. The maximum electron energy in the measured Roentgen ray spectrum corresponds to the inter-electrode voltage. The system was calibrated using two standard radiation source [241]Am and [152]Eu. After adjusting the amplification factor properly, γ ray of [241]Am 59.54 keV locates at channel 316 while [152]Eu 344.31 keV at channel 1889, then two peaks appear at channel 661 and channel 1340 corresponding to [152]Eu 121.78 keV and [152]Eu 244.66 keV, respectively. The above 4 points fit a well linearity, which means the calibration is successful.
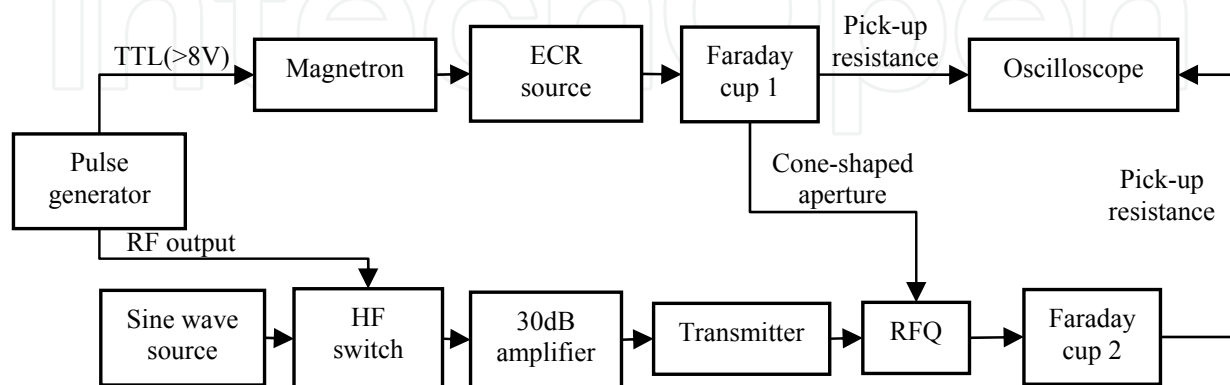
Fig. 15. The rf and measurement system of the experiment for the ladder IH-RFQ.

From the measured Roentgen spectrum at rf power 26.4 kW as shown in Fig.16, it can be found that the inter-electrode voltage reaches 72.1 kV, which is higher than the required value 60 kV. What should be paid attention to is that the spectrum was measured at the glass window locating near the entrance of the RFQ. According to Fig.14, the inter-electrode voltage unflatness is about ±7%, as a result, the average value of it along the cavity longitudinally should be 72.1/1.07 kV, i.e. 67.3 kV in this power case. All the measured voltages are normalized in this way. Figure 17 plots the variation of the square of the inter-electrode voltage with rf power, from which it can be seen that the linearity is well. The specific shunt impedance is defined as $R_s = (V^2/P) \cdot L = R_p \cdot L$, where L=1123 mm is the length of the RFQ. The slope of the fitting line that means the shunt impedance is 162 kΩ, so the corresponding specific shunt impedance is 178 kΩ•m. The result is better than that of simulation and cold measurement, which is because that the conductivity was set to be 5.0×10^7 S/m not 5.9×10^7 S/m in MWS simulations and the rf properties were improved via advance power test. The temperature of cooling water increased from 15.7 °C to 23.4 °C while the rf power increasing from 0 to 29.7 kW, and no sparking phenomenon appeared during the experiment. The results above indicate that the RFQ cavity possesses well mechanical strength and is water-cooled effectively.

The beam test has been performed using [4]He^{+} beam. The output current and transmission efficiency of the ladder IH-RFQ varying with the rf power fed into it are shown in Fig. 18 when the extraction current from the ECR source is 30 μA. The maximum transmission efficiency reaches 70%. During the experiment, the highest output beam is 210 μA, and the transmission efficiency is better than 70% at current of several tens μA. It should be figured out that the transmission efficiency is mainly limited by the unmatched beam injected to the RFQ, especially for high current beam. Further efforts will be made to improve it. The following works will also include the beam test of heavier ions, measurement of the energy spectrum, and some application studies on the RFQ as an implanter.
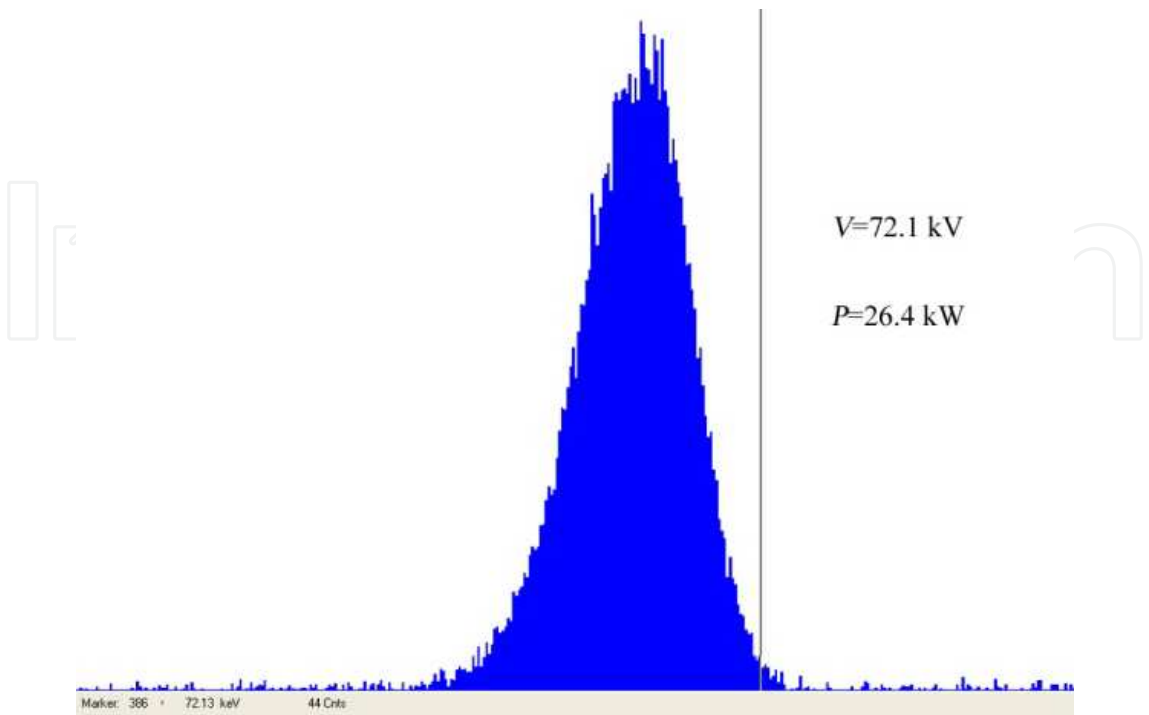
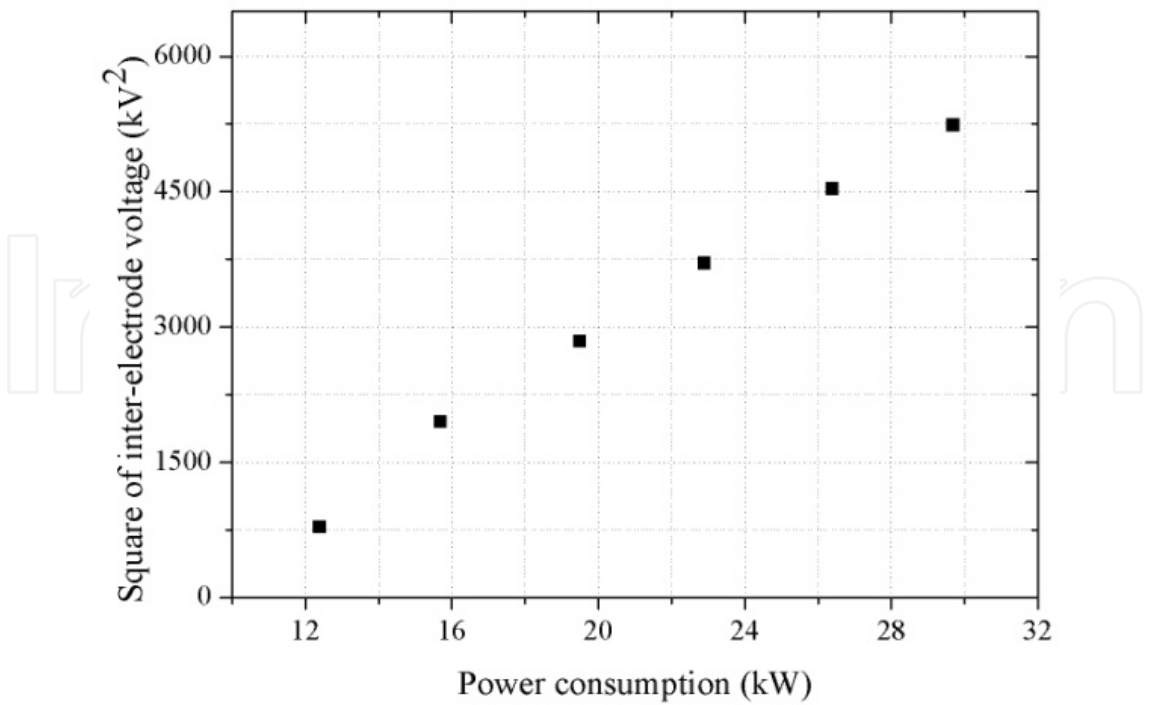Fig. 16. Roentgen spectrum at 26.4kW rf power.

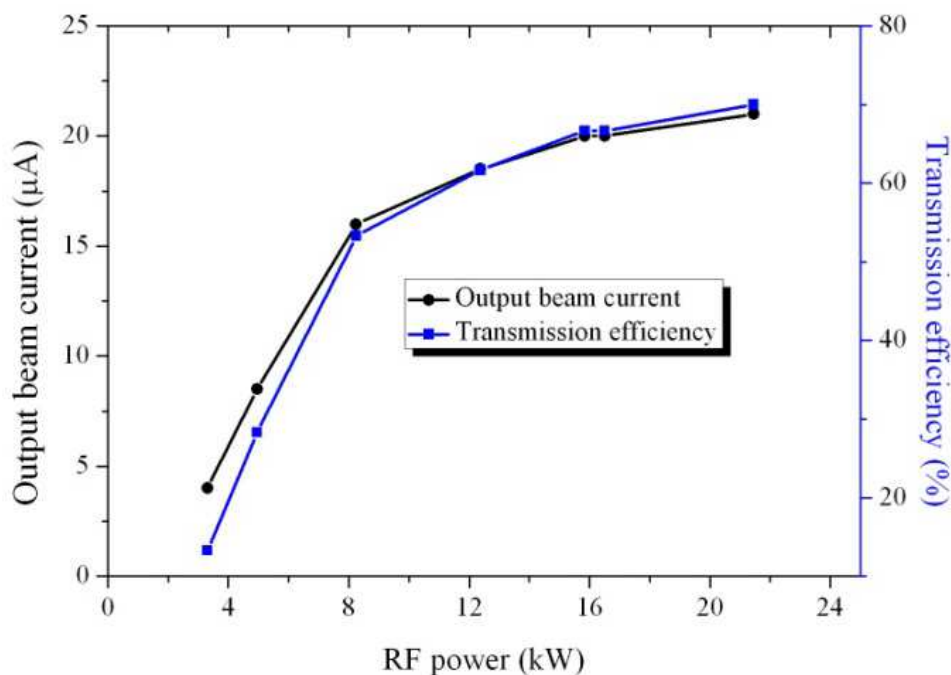Fig. 17. Square of the inter-electrode voltage vs rf power.

Fig. 18. The output current and transmission efficiency of the RFQ vs rf power at the extraction current 30μA(^{4}He$^+$)

6. Summary

In conclusion, the RFQ accelerator is a competent ion implanter with many advantages such as high energy (MeV), high current (μA-mA), variable energy and ion species, compact size and so on. Further studies will be made on the practical usage of the RFQs in the ion implantation field. As for the ladder IH-RFQ accelerator of Peking University, after the further beam test is finished, some ion injection experiment will be made for the surface modification of materials.

7. Acknowledgement

8. References

[1] M. Kapchinsky, V. A. Teplyakov, Linear Ion Accelerator with Spatially Homogeneous Strong Focusing, Prib. Tekh. Eksp., 1970, No.2, p.19.
[2] T. P. Wangler, Principles of RF Linear Accelerators, Wiley Series in Beam Physics and Accelerator Technology, 1998, p.225-257.
[3] H. Klein, Development of the Different RFQ Accelerating Structures and Operation Experience, IEEE Trans. Nucl. Sci., 1983, Vol. NS-30, p.3313.

[4] L. Young, 25 Years of Technical Advances in RFQ Accelerators, Proc. of PAC2003, p.60.

[5] A. Schempp, Research application of RFQ linac, Nuclear Instruments and Methods in Physics Research Section B, 1995, Vol.99, p.688-693.

[6] Ren Xiao-Tang, Lu Yuan-Rong, Yu Jin-Xiang, et al., Experimental research on simultaneous acceleration of positive and negative ions with equal q/m in an ISR RFQ, High Energy Physics and Nuclear Physics (in Chinese), 2000, Vol.24, p.347-351.

[7] U. Ratzinger, et al., The GSI 36 MHz high-current IH-type RFQ and HIIF-relevant extensions, Nuclear Instruments and Methods in Physics Research Section A, 1998, Vol.415, p.281-286.

[8] Y. R. Lu, C. E. Chen, J. X. Fang, et al., Investigation of high duty factor ISR RFQ-1000, Nuclear Instruments and Methods in Physics Research Section A, 2003, Vol.515, p.394-401.

[9] Kensuke Amemiya, Junya Ito and Katsumi Tokiguchi, Aluminum ion implantation using a variable energy RFQ implanter, Proc. of EPAC1998, p.2419.

[10] Byung-Wuek Lee, Jong-Won Kim and Holger Podlech, Design study of an RFQ for high-energy ion implantation, Journal of the Korean Physical Society, 2006, Vol.48, p.810-814.

[11] A. Schempp, et al., High duty factor nitrogen RFQ as a prototype high current implanter, Nuclear Instruments and Methods in Physics Research Section B, 1998, Vol.139, p.411-417.

[12] Zhiyu Guo, et al., Feasibility studies of RFQ based ^{14}C accelerator mass spectrometry, Nuclear Instruments and Methods in Physics Research Section B, 2007, Vol.259, p.204-207.

[13] NIE Yuan-Cun, LU Yuan-Rong, CHEN Jia-Er, et al., Theoretical design of a 104 MHz ladder type IH-RFQ accelerator, Chinese Physics Letters, 2010, Vol.27, p.112901.

[14] Fang Jiaxun, et al., RFQ accelerators for ion implantation, Nuclear Techniques (in Chinese), 2006, Vol.29, p.140-144.

[15] J. W. Staples, Reducing RFQ Longitudinal Emittance, Proc. of LINAC1994, p. 755.

[16] K. R. Crandall, R. H. Stokes, T. P. Wangler, RF quadrupole beam dynamics design studies, Proc. of LINAC1979, BNL-51134, p.205.

[17] X. Q. Yan, et al., Matched and equipartitioned design method for modern high-intensity radio frequency quadrupole accelerators, Nuclear Instruments and Methods in Physics Research Section A, 2007, Vol.577, p.402-408.

[18] www.cst.com

[19] H. Podlech, et al., Electromagnetic design of an 80.5 MHz RFQ for the RIA driver Linac, Proc. of EPAC2002, p.942-944.

[20] R. M. Hutcheon, An equivalent circuit model of the general 3-dimensional RFQ, IEEE Trans. Nucl. Sci., 1983, Vol. NS-30, p.3524-3526.

[21] J. X. Fang, and A. Schempp, Equivalent circuit of a 4-Rod RFQ, Proc. of EPAC92, p.1331-1333.

[22] J. Schmidt, et al., Tuning of the 4-Rod RFQ for MSU, Proc. of IPAC'10, p.762-764.

[23] P. Fischer and A. Schempp, Tuning of a 4-rod cw-mode RFQ accelerator, Proc. of LINAC06, p.728-730.

[24] P. G. Bricault, Methods for measurement of the specific shunt impedance of RFQ, TRIUMF DESIGN NOTE TRI-DN-94-30, 1994.

[25] Lu Yuan-Rong, Chen Wei, Nie Yuan-Cun, et al., Power test of the ladder IH-RFQ accelerator at Peking University, Chinese Physics Letters, 2011, Vol.28(7), p.072901.

[26] M. Zhang, S. X. Peng, Z. Z. Song, et al., Experimental results of an ECR oxygen source and a LEBT system for 1 MeV ISR RFQ accelerator upgrade project, Chinese Physics C, 2008, Vol.32(Suppl.I), p.220-222.
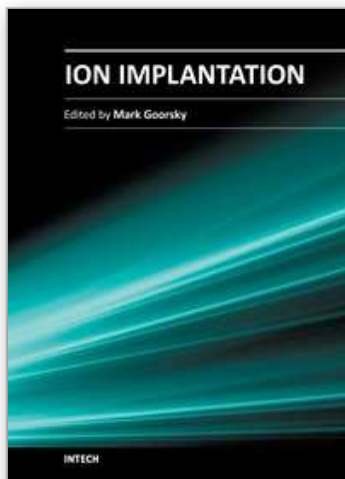
Ion Implantation

Edited by Prof. Mark Goorsky

Ion implantation presents a continuously evolving technology. While the benefits of ion implantation are well recognized for many commercial endeavors, there have been recent developments in this field. Improvements in equipment, understanding of beam-solid interactions, applications to new materials, improved characterization techniques, and more recent developments to use implantation for nanostructure formation point to new directions for ion implantation and are presented in this book.

How to reference

In order to correctly reference this scholarly work, feel free to copy and paste the following:

Yuancun Nie, Yuanrong Lu, Xueqing Yan and Jiaer Chen (2012). Radio Frequency Quadrupole Accelerator: A High Energy and High Current Implanter, Ion Implantation, Prof. Mark Goorsky (Ed.), ISBN: 978-953-51-0634-0, InTech, Available from: http://www.intechopen.com/books/ion-implantation/radio-frequency-quadrupole-accelerator-a-high-energy-and-high-current-implanter

INTECH
open science | open minds